Rikio Maruta was born on May 15, 1943. He graduated from the Nippon Electric Institute of Technology in 1967, where he majored in electrical engineering. From 1968 to 1969, he was a research student at the University of Tokyo.

He has been an employee of Nippon Electric Company, Ltd. since 1962. His principal job has been research and development of high-speed PCM multiplexers and digital signal processing terminals such as digital speech interpolation equipment and TDM/FDM transmultiplexers. He was awarded the 1976 Conference Paper Award by the Institute of Electronics and Communication Engineers (IECE) of Japan, and the 1978 Kanto Regional Invention Award by the Japan Institute of Invention and Innovation. He is presently Supervisor, Communication Research Laboratory, Central Research Laboratories, Nippon Electric Company, Ltd.

Mr. Maruta is a member of the Institute of Electric Engineers (IEE) of Japan and the Institute of Electronics and Communication Engineers (IECE) of Japan.

Atsushi Tomozawa was born in Tokuyama, Yamaguchi, Japan, on January 6, 1938. He received the B.S. degree in electrical communication engineering from the Kyushu University in 1960.

He joined the Nippon Electric Company, Ltd. in 1960, and has worked on research and development of PCM systems including delta modulation, high-speed codecs, and digital multiplexers at the Central Research Laboratories. From 1971 through 1974, he was engaged in system studies on TDMA and digital signal processing at COMSAT Laboratories. He was awarded the 1965 Inada Prize by the Institute of Electronics and Communication Engineers (IECE) of Japan. He is presently Assistant Manager, Digital Systems Development Department, Transmission Division, Nippon Electric Company, Ltd.

Mr. Tomozawa is a member of the Institute of Electronics and Communication Engineers (IECE) of Japan.

Prediction of Attenuation by Rain

ROBERT K. CRANE, FELLOW, IEEE

Abstract—**A new model is presented for the prediction of attenuation by rain on either terrestrial or slant earth-to-space propagation paths. The model was developed using geophysical observations of the statistics of point rain rate, of the horizontal structure of rainfall, and of the vertical temperature structure of the atmosphere. The model was tested by comparison with attenuation distribution observations. The results show excellent agreement; the observations differ from model predictions by less than the rms deviations predicted by the model.**

I. INTRODUCTION

RAIN has long been recognized as one of the principal causes of unwanted signal loss on centimeter or millimeter wave propagation paths through the lower atmosphere. Rain is not the only cause. Variations in water vapor along a path or the occurrence of liquid water clouds or fog on the path will also cause variations in signal strength. Fig. 1 displays the relative magnitude of the variations (attenuation) due to water vapor (gaseous absorption), a liquid water cloud, and rain that is expected to be exceeded during less than 2 percent of the year on a zenith path. Specifically, the curves for gaseous absorption display the estimated global variation (two standard deviations) of attenuation about the global and seasonal mean value of attenuation and the variation about the attenuation value computed for a given surface temperature and water vapor density; the cloud values are for a 2 km thick cloud with a 0.2 g/m^3 liquid water content; and the rain curve is for a 2.5 km high rain region of 1 mm/h, conditions typical of the rain rate to be exceeded 2 percent of the year at 38°N latitude along the eastern United States. With the exceptions of the frequency bands about the 22 GHz water vapor absorption line and the 60 GHz complex of oxygen lines, the attenuation exceeded less than 2 percent of the year is caused by rain or cloud. The model cloud produces an attenuation estimate comparable to rain at 2 percent of the year. At the smaller percentages of the year of interest to the communication system designer, rain is the sole cause of increased attenuation.

Early recognition of the importance of rain to systems designed for service reliabilities in excess of 0.99 led to a number of theoretical and experimental studies of the effects of rain. By the early 1970's, a firm theoretical basis had been established for the calculation of attenuation if the rainfall intensity was known along the path [1], [2]. In recent years, the emphasis has been on establishing predictive techniques for the statistical estimation of the attenuation probability distribution for a particular path. Two different approaches to the

Paper approved by the Editor for Communication Theory of the IEEE Communications Society for publication without oral presentation. Manuscript received October 2, 1979; revised January 30, 1980. This work was supported by contracts from the NASA Goddard Space Flight Center, Western Union Telegraph Company, and M.I.T. Lincoln Laboratory.

The author is with Environmental Research & Technology, Inc., Concord, MA 01742.

0090-6778/80/0900-1717$00.75

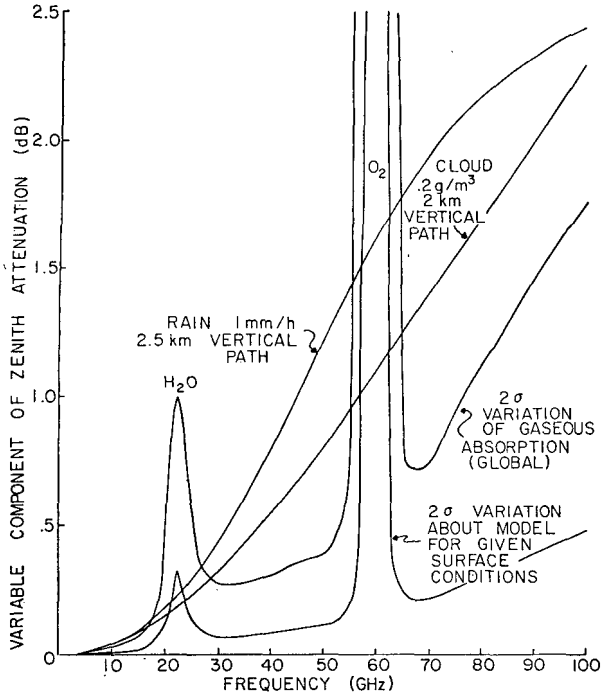

Fig. 1. Zenith attenuation values expected to be exceeded 2 percent of the year at midlatitudes.

estimation problem are possible, one based solely on the use of a large number of attenuation observations at differing frequencies, locations, and path geometries, and the other based on the synthesis of attenuation values from meteorological data. The latter is most promising at the current time because a considerably larger database is available for use in estimating the distribution functions required for modeling path attenuation.

The statistical variations of rainfall intensity, specific attenuation, and attenuation along a path depend in a complex way on the number, type, and intensity of rainstorms that traverse the path each year. No theoretical basis exists for the calculation of the desired rainfall statistics; they must be obtained empirically. Rice and Holmberg [3] performed a statistical analysis of all the then available U.S. National Weather Service rain accumulation observations to provide estimates of instantaneous rain rate distributions. Lee [4] has since published a similar, although less extensive, analysis of the same data. He described the available data and proposed a procedure for the estimation of the desired rain rate statistics. Dutton and Dougherty [5] have extended the work of Rice and Holmberg to provide estimates of the year-to-year variability of the rain rate distribution.

More than an estimate of the surface point rain rate distribution is required for the prediction of attenuation on terrestrial or earth-to-space (slant) communication paths. Rain displays significant spatial and temporal variation along a horizontal path, and procedures are required to statistically estimate the instantaneous rain rate profile along the path. Battesti *et al.* [6], Lin [7], Stutzman and Bostian [8], Rogers [9], and a number of others have proposed models for the calculation of attenuation along a path given the equal probability rain rate value at a point. The models are based either on a direct empirical relationship between surface rain rate and an effective path length which, when multiplied by the specific attenuation value for the surface rain rate, produces the desired attenuation value [6] or on a synthetic storm profile which is used to represent the variation of rain along the path. Most of the models were developed using point rain rate and path attenuation measurements; the free parameters in the model are set to provide the best match between the attenuation estimated using the prediction procedure and the observed values. Model rainstorms have also been developed from analyses of weather radar data for the conversion of point rainfall statistics to path attenuation estimates [9].

Finally, for the prediction of attenuation on a slant path, the vertical variation in rain intensity and in ice or a water state must be modeled. At frequencies below 60 GHz, the attenuation caused by frozen particles such as snow or ice crystals is very small and may be neglected [10]. Only the contribution of the liquid raindrops is important. Observations of the variation of specific attenuation with height reveal that the region producing significant attenuation lies below the height of the bright band (0°C isotherm) [11]; comparisons between radar-based attenuation predictions and simultaneous path attenuation measurements also indicate that only the rain below the bright band contributes to the attenuation [12], [13]. Weather radar observations show that, on average, the rain intensity does not vary with height between the surface and the base of the bright band [14], [15]. On the basis of this evidence, the specific attenuation may be modeled as being constant from the surface to a height near the 0°C isotherm level which must also be statistically estimated.

An attenuation prediction model based upon the use of geophysical data incorporates predictions of the surface point rain rate, the point-to-path variation in rain rate or specific attenuation given the surface point rain rate, and the height dependency of specific attenuation given the surface point rain rate or the percentage of the year the attenuation value is exceeded. This paper presents such a model for use on either slant or terrestrial paths. It is based entirely on geophysical observations of rain rate, rain structure, and the vertical variation of atmospheric temperature. None of the model constants was obtained from attenuation measurements. This procedure was used to amass as large a database as possible from pooled observations at a number of locations. Crane [10] showed that over 10 years of observation at a point are required to estimate the surface rain rate to be exceeded 0.001 percent of the year on the average with an uncertainty (1 standard deviation or 67 percent bound) of less than 10 percent of the estimated value. No equivalent long term attenuation data are currently available from a single location for use in generating a prediction model.

An attenuation prediction model should also provide estimates of the expected year-to-year and the expected station-to-station variation as well as the expected attenuation at the same exceedence probability. The model presented in this paper includes such estimates for either terrestrial or slant paths. Comparisons between model predictions and available attenuation observations made on a number of propagation paths show agreement within the expected uncertainty. The predic-

tion procedure for point rain rate is developed in Section II, the horizontal variation in rain rate and specific attenuation in Section III, the vertical variation of specific attenuation in Section IV and the expected variation of the estimated values in Section V. Comparisons with observations are presented in Section VI.

II. PREDICTION OF SURFACE POINT RAIN RATE

Distribution at Fixed Location

No physical theory exists for the calculation of a surface point rain rate distribution. Consequently, distribution estimates are empirical and must be developed from the available long-term observations of rain accumulation. Two types of rain accumulation data exist: the long duration hourly, daily, and annual accumulation tabulations available for a large number of geographical locations, and the excessive precipitation data available from a limited number of locations [4]. Nearly instantaneous rain rate data are available for an extremely limited number of locations and for limited time durations, typically of a few years or less. The instantaneous data have generally been taken in conjunction with attenuation observations, and provide a comparison for model evaluation, but not a database suitable for establishing the expected rain rate distribution.

A larger database of nearly instantaneous observations is potentially available in the archives of the U.S. National Weather Service in the form of unanalyzed strip chart recordings. Bodtmann and Ruthroff [16] obtained and analyzed data for five years of observations at 20 locations in the United States. The time resolution of the data, however, was limited; the observations represented rain rate values averaged over time intervals on the order of 2–4 min. For the estimation of attenuation along a path, the specific attenuation at each point along the path is required. The specific attenuation is theoretically related to the instantaneous rain rate using measured or modeled raindrop size distributions. Because of the instantaneous/point nature of the data fields needed for the nonlinear rain rate to specific attenuation conversion, it is often assumed that only instantaneous rain rate distributions are useful in the prediction of attenuation. Truly instantaneous rain rate measurements are contaminated by fluctuations caused by atmospheric turbulence and, if the sampling area is small, by the stochastic variation produced by counting a number of raindrops of different sizes and fall velocities. Rain rate averages are needed to remove the variations due to gauge limitations and to turbulence.

The amount of averaging desirable in the preparation of a rain rate distribution estimate depends upon its application. Bussey [17] noted the equivalence between temporal and spatial averaging for translating rain cells and recommended the use of hourly averages for the estimation of attenuation on 50 km terrestrial paths. Radar observations show that rain cells defined by regions of high rain rate which cause significant attenuation have an average dimension of 3 km measured at 60 percent of the peak rain rate value [18]. Assuming an average translation velocity of 15 m/s, a rain cell will pass over a rain gauge in less than 4 min. A rain gauge with a 1–2 min time resolution will resolve the small but significant cells; gauges with longer averaging times will miss the peaks of the cells. For the prediction of attenuation on a variety of terrestrial or slant paths, a 1 min accumulation or averaging time is optimum.

Except for a very limited number of recorded "instantaneous" rain rate distribution observations, 1 min accumulation data are not available. Rice and Holmberg [3] and Lee [4] have devised approximation procedures for the estimation of instantaneous rain rates from the available excessive precipitation data. The excessive precipitation data reported through 1972 consist of the highest 5 min, 10 min, and longer accumulations from each storm with an average 5 min rain rate in excess of 76.2 mm/h, an average 10 min rain rate in excess of 45.7 mm/h, and lower thresholds for longer accumulation periods. In 1972, the excessive precipitation criteria were changed to record only the highest accumulation event each month. If two occurrences of excessive precipitation happen within a storm, only the highest is recorded. Currently, if two events occur within the same month, only the highest is recorded. These data are useful for estimating the highest 5 min accumulation per month and per year, but are of limited use for the direct estimation of annual rain rate statistics valid at 10 min per year or longer. Both Rice and Holmberg and Lee devised models for the use of the data. Comparisons between the Rice-Holmberg model predictions and available instantaneous data show that their model tends to overestimate the rain rates at 0.01 percent and smaller percentages of the year [15].

Measured and modeled rain rate distributions for Washington, DC are presented in Fig. 2. The measured distributions are for one year of data as reported by Bussey [17] and for two years of data measured in Greenbelt, MD [19]. The instantaneous data obtained by Bodtmann and Ruthroff for their location nearest to Washington, DC is also plotted, as is the model prepared by Lee and used by Lin [7]. The Lin-Lee model was empirically adjusted during its development to match the Bodtmann and Ruthroff observations. The model predictions produced by Rice and Holmberg and as refined by Dutton and Dougherty are also presented. As noted above, the Rice-Holmberg model overestimated the rain rate at 0.01 percent of the year.

Rice and Holmberg processed both the excessive precipitation data and the hourly data available from the National Weather Service, Experience with varying the integration interval for processing instantaneous rain rate data has shown that averaging affects only the higher rain rates at the smaller percentages of the year [9], [10], [20]. In the 0.1–1 percent of the year interval, the distribution function for hourly observations provides a good estimate of the distribution function for 1 min averaged rain rate. The Rice-Holmberg model, therefore, should provide a good estimate of the rain rate distribution in the 0.1–1 percent range, a result which is evident in Fig. 2.

The highest 5 average rain rate value in the figure was obtained from the excessive precipitation data for the 26 year period from 1950 through 1976. These data were processed to provide estimates of the mean and standard deviation of the

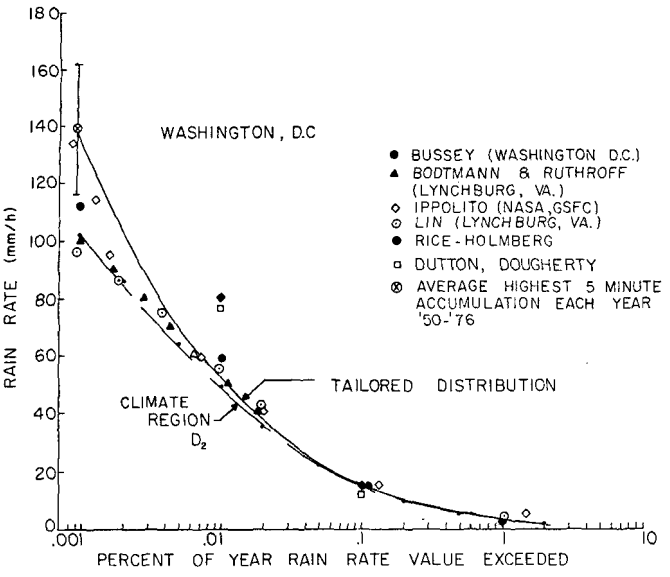

Fig. 2. Measured and modeled instantaneous rain rate distribution for Washington, DC.

rain rate to be exceeded 5 min of the year (~0.001 percent). Analysis of instantaneous rain rate distributions have shown that the highest 5 min average rain rate is usually from an excessive precipitation event that includes the five highest 1 min averaged rain rate values. Assuming this equivalence, the rain rate distribution is known at 0.00095 percent of the year (5 minutes) and in the 0.1-1 percent range (from the Rice-Holmberg model). The tailored distribution plotted in Fig. 2 is a smooth curve that passes through the known values. This curve represents the best estimate available based upon a long data sample. At 0.001 of the year, the observed standard deviation of rain rate values for Washington, DC was 17 percent. The measured distribution reported by Bussey falls just outside this range and the distribution reported by Ippolito falls within this range (rms) about the tailored distribution. Similar agreement is obtained at the other probability of occurrence extreme, 1 percent of the year: the measurements are within the expected 17 percent rms of the tailored and the climate region D_2 model distributions.

Regional Model

Data for the preparation of tailored distributions are only available from First Order Weather Stations in the United States [4] and at a limited number of additional stations throughout the rest of the world. Attenuation predictions are generally required for locations different from the limited number of stations with sufficient long-term data. Crane [10], in processing excessive precipitation data from 15 stations in New England and Eastern New York State, found that the mean and variance of data pooled from seven years and 15 stations were statistically identical with the mean and variance for 24 years at one of the stations (Boston). The mean rain rate was 100 mm/h and the standard deviation was 35 percent for the 15 station sample, and the mean rain rate was 91 mm/h and the standard deviation was 48 percent for Boston. The distribution function for the highest 5 min average rain rate accumulation per year for Boston was applicable to the New England, Eastern New York region. This result implies that regional maps are useful for the representation of rain rate distribution data for application to locations removed from the observing station. The result also suggests the use of data pooled from a region to provide improved statistical estimates for the distribution function.

Rice and Holmberg [3], in the development of the empirical parameters and their dependences on total rain accumulation and thunderstorm rain accumulation, pooled data from stations within each of the 10 climate regions defined by Barry and Chorely [21] for the United States. The climate regions were defined on the basis of temperature, terrain height, average rain accumulation, and vegetation type, not on the basis of similarity in rain rate distribution. A subsequent comparison of the model distribution functions produced for each climate region resulted in the reduction of the number of rain climate regions required to describe the pooled rain rate distributions to five, the five climate regions currently employed by the CCIR [22]. These climate regions, although fashioned for the United States, were subsequently employed to describe rain climate regions for the entire globe. Dutton [23] has since expanded the number of rainfall zones in the United States to 19 based upon mappings of the independent parameters in the Rice-Holmberg model.

The global model currently used by the CCIR represents rain climates typical of those found within the United States, but does not adequately represent the much more intense rain rate regime found in the wet tropical regions of Africa, South America, and Indonesia or the much less intense regime found in the Arctic. In the development of a new global rain climate model for use in communication system design, the number of regions chosen to represent the variation in rain rate was expanded from five to eight to better emphasize variation with latitude. The newly developed rain rate climate model is presented in Figs. 3 and 4. The United States is still spanned by five regions, although one of the regions is divided into three subregions to better describe the within-region climate variation for design application.

The climate region boundaries were established using total rain accumulation and the number of thunderstorm day maps provided by the World Meteorological Organization as published in the *World Survey of Climatology* series edited by Landsberg [24]. In data-sparse regions, guidance was taken from the Köppen world climate classification [25] which, although heavily based upon vegetation type, represents major variations in rain climate. The ranges of the total rain accumulation and thunderstorm day values used for the definition of the rain climate regions were obtained from an initial analysis using the Rice-Holmberg model for Europe and North America. The initial intent was to define rain rate regions with rain rate distributions for adjacent regions approximating the expected bounds for the temporal (year-to-year) and spatial variation of the rain rate distribution within a region; the median rain rate distribution values for each climate region were to differ by approximately 40 percent at 0.001 percent of the year.

The boundaries for each of the climate regions were adjusted

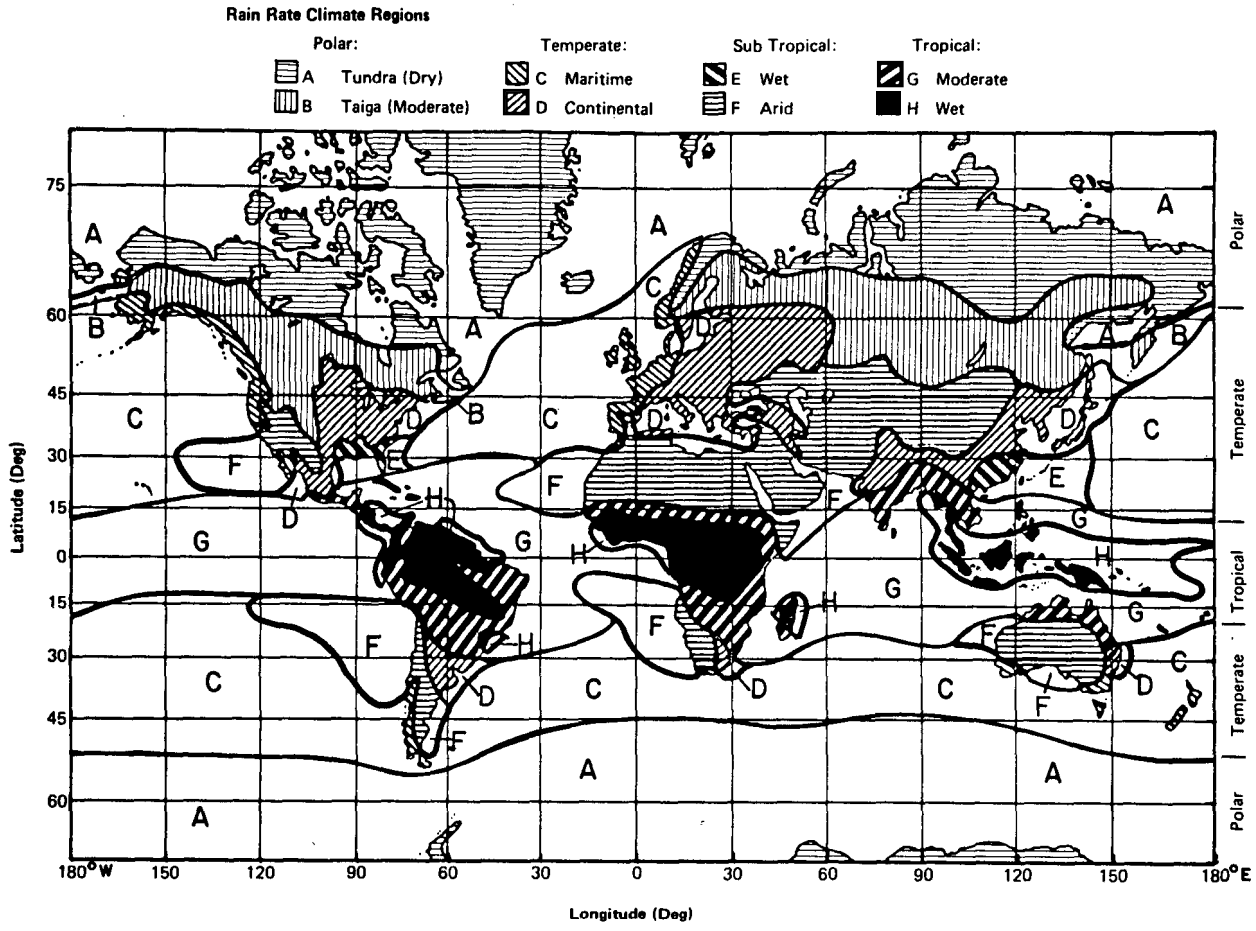

Fig. 3. Rain rate climate regions.

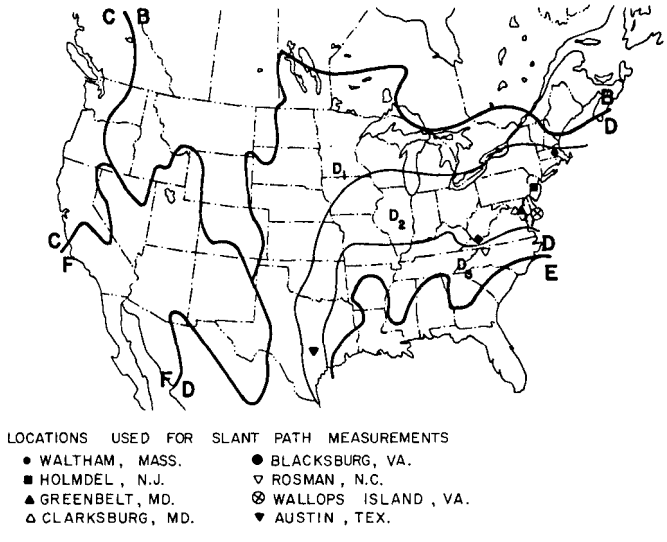

Fig. 4. Rain rate climate regions within the United States.

to compensate for the expected variations caused by terrain, variations in the predominant storm type, storm motion, and general circulation of the atmosphere, and the dominant latitude variation in rain climate. In addition, satellite cloud data, microwave radiometer observations of rain rate [26], and precipitation frequency data [27] were used to extend the rain climate regions out over the oceans.

The available measured instantaneous rain rate distributions were pooled for each of the climate regions defined in Fig. 3 and used to construct a median rain rate distribution for the region. No data were available for Region A, 132 station-years of data were available for Region D_2, and intermediate numbers of station-years were available for the other regions (see Table I). The resulting distributions for each of the eight climate regions are depicted in Fig. 5; the empirical distribution function for Region H together with the measured distributions used for the preparation of the model distribution are presented in Fig. 6. The rain rate distributions are also given in Table I for convenient reference.

Region D, as a result of the refinements used to prepare the final distributions, spans a large range of rain rates at a given exceedence probability. For application within the United States, Region D is bounded by Region E to the southeast and by Regions B or F to the north and west. At 0.001 percent of the year, the expected rain rates range from 64 to 164 mm/h, +61 to −37 percent relative to the 102 mm/h value for Region D. This range is too large for system design, although it is in reasonable accord with the expected standard deviation of 33 percent for one year of observations calculated using 26 years of excessive precipitation data from eight First Order Weather Stations within climate Region D. Region D was divided into three subregions, as shown in Fig. 7, to provide an interpolation of the expected rain rate distributions within the climate

TABLE I
POINT RAIN RATE (R_p) DISTRIBUTION VALUES (mm/h) VERSUS PERCENT OF YEAR RAIN RATE IS EXCEEDED

Percent of Year	Rain Climate Region									
	A	B	C	D_1	D_2	D_3	E	F	G	H
0.001	28	54	80	90	102	127	164	66	129	251
0.002	24	40	62	72	86	107	144	51	109	220
0.005	19	26	41	50	64	81	117	34	85	178
0.01	15	19	28	37	49	63	98	23	67	147
0.02	12	14	18	27	35	48	77	14	51	115
0.05	8.0	9.5	11	16	22	31	52	8.0	33	77
0.1	5.5	6.8	7.2	11	15	22	35	5.5	22	51
0.2	4.0	4.8	4.8	7.5	9.5	14	21	3.2	14	31
0.5	2.5	2.7	2.8	4.0	5.2	7.0	8.5	1.2	7.0	13
1.0	1.7	1.8	1.9	2.2	3.0	4.0	4.0	0.8	3.7	6.4
2.0	1.1	1.2	1.2	1.3	1.8	2.5	2.0	0.4	1.6	2.8
Number of Station Years of Data	0	25	44	15	99	18	12	20	2	11

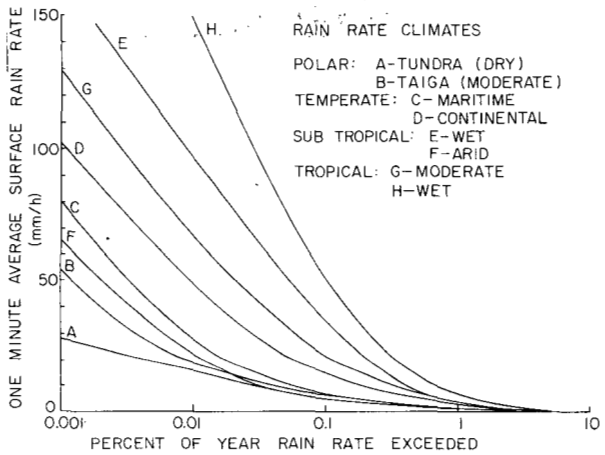

Fig. 5. Model rain rate distribution functions for the climate regions of Fig. 3.

region. The Region D_2 measurements displayed in Fig. 7 were not used in the derivation of the D_1, D_2, or D_3 model curves, but are provided for an independent evaluation of the subregion distribution bounds.

Further subdivision is possible, but depends upon the availability of adequate rain rate data and upon a better understanding of the local effects of terrain and of regional storm types and motions. Further subdivision, while producing better average values for system design, would not simultaneously display the approximate year-to-year variation in the values. The year-to-year variability is modeled as 30 percent of the expected value at the distribution extremes, 0.001 and 1 percent of the year (see Fig. 7). At the intermediate values, 0.01 and 0.1, the uncertainty is reduced to 20 percent to match the results reported by Harden *et al.* [28]. The spatial and temporal variability reported by Harden *et al.* for the United Kingdom (UK), together with the climate Region *C* model curve and bounds, are presented in Fig. 8. The UK data summarized in Fig. 8 were not used in the derivation of the climate Region *C* distribution function. These data show reasonable agreement with the model, although the model tends to overpredict the rain rate in the UK at 0.001 percent of the year. Since the data reported by Harden *et al.* were obtained from gauges with a 2 min time resolution, the discrepancy may be due to the climate or due to gauge limitations.

The rain climate model presented in Figs. 3, 4, 5, and 7 provide the rain rate distribution data needed for the estimation of attenuation. The regions were chosen to span areas with roughly identical year-to-year and location-to-location variations in rain rate distribution values. For a better representation of the rain rate distribution to be expected on the average at a point, a tailored distribution can be prepared (within the United States) using excessive precipitation data from nearby First Order Weather Stations for 0.001 percent of the year and the model calculations prepared by Rice and Holmberg [3] for percentages of the year greater than 0.1 percent. Care should be exercised in using a tailored model since local variations may compromise the expected increase in model precision. Refinement using measured instantaneous rain rate distributions is not recommended due to the expected year-to-year variation in the measured values and the current lack of measurements spanning time intervals of 10 or more years.

III. PREDICTION OF RAIN RATE AND SPECIFIC ATTENUATION ALONG A PROPAGATION PATH

A model for the prediction of surface point rain rate is only the first step in a model for the prediction of attenuation. Rain is characteristically inhomogeneous in the horizontal, and a statistical model is required to provide an estimate of the effect of the inhomogenity on the estimation of attenuation. For application to attenuation modeling, rain is often divided into two classes, stratiform and convective. Weather radar observations reveal that stratiform or widespread rain generally contains regions of imbedded convection and convective cells that are often surrounded by more stratiform regions of lighter rain [14]. Crane [18] has found a marked similarity in the underlying structure of both widespread and showery rain. The rain cell sizes and spacings observed by radar in widespread and isolated shower conditions on the Kansas high plains are identical to those observed in widespread rain in Coastal Virginia. The cell sizes also match those observed in Switzerland, France, Japan, and Malaysia [22].

In the semi-empirical modeling of fluid flow, similar results are expected for situations characterized by the identical values of nondimensional parameters such as the Prandlt number, the Reynolds number, the Rayleigh number, etc. In application to convection in the atmosphere, the fluid dynamical parameters used to characterize the flow are only weakly dependent on climate; hence, the horizontal structure of rain should not depend on climate region. Data on rain cell size, spacing, and the conditional point-to-path variation in rain rate, therefore, can be pooled from different geographic locations and rain climate regions.

Although radar provides the ideal tool for observing the spatial structure of rain [10], insufficient radar data are available to provide a conditional point-to-path relationship. Suf-

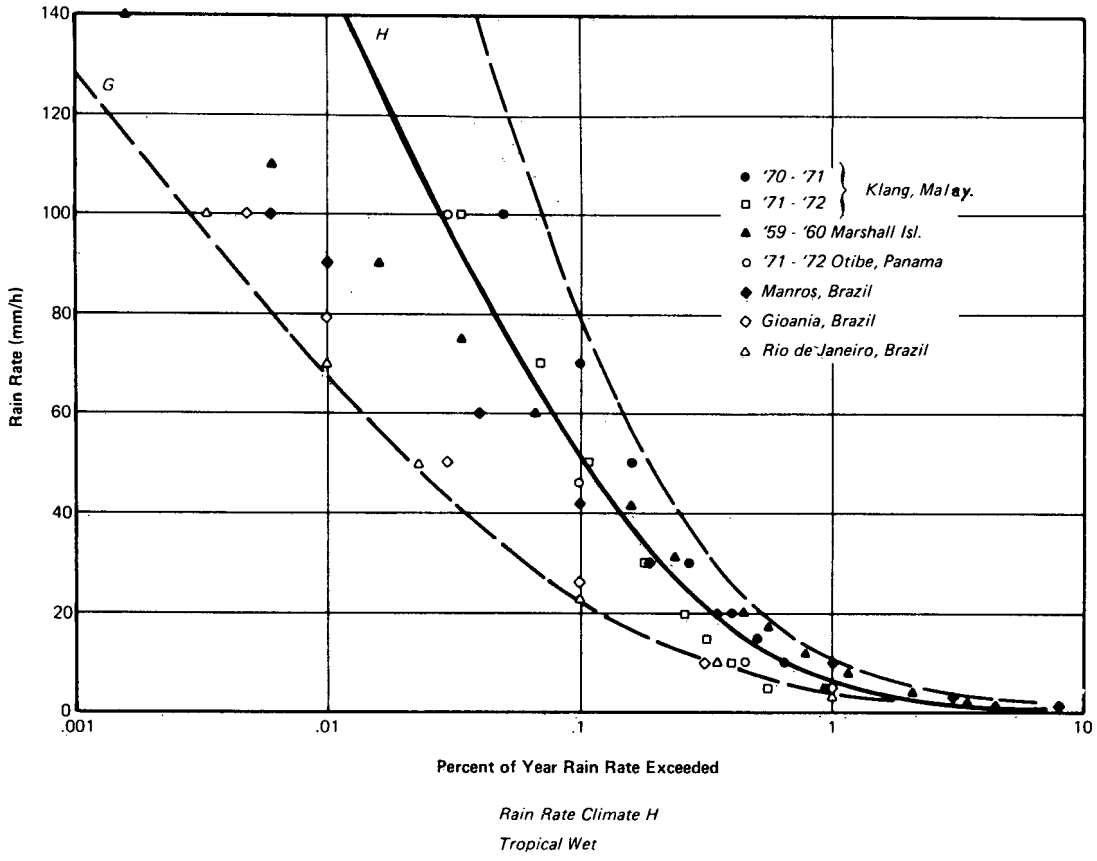

Fig. 6. Rain rate distribution observations for climate Region *H*.

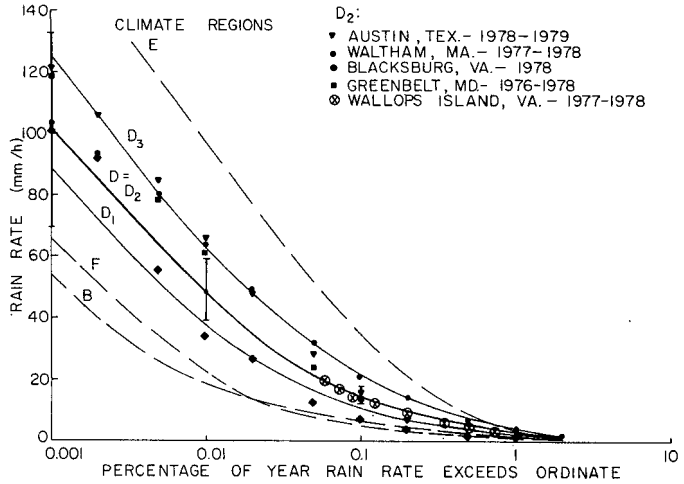

Fig. 7. Rain rate distributions for climate Region *D* within the United States (Fig. 4).

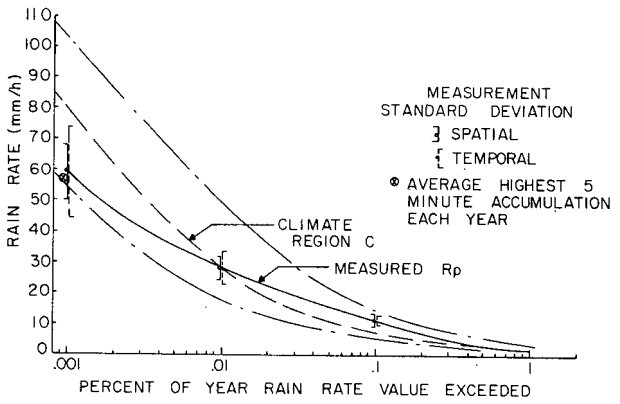

Fig. 8. Rain rate distribution observations in the United Kingdom [28].

ficient data, however, are available from a limited number of rain gauge networks. Jones and Sims [20] reviewed the Thunderstorm Project rain gauge network measurements (obtained in 1946) and more recent data from England to obtain relationships between point and path averaged rain rate values at equal exceedence probabilities. Data were also available from a dense rain gauge network operated for a limited time period by Bell Laboratories in New Jersey [29] and from a line of gauges along a 20 km path in the Rhine Valley of West Germany [30]. These data were pooled to provide an empirical relationship between point and path average rain rate as depicted for a distance of 5 km in Fig. 9.

The path averaged rain rate was plotted versus surface point rain rate for equal exceedence probabilities. Surface rain rate was used as the independent variable rather than probability because the rain rate values are a better measure of rain intensity (hence the dynamics of the meteorological situation that produced the rain) than is percentage of the year when the data are pooled from a number of climate regions. The path average value is expressed as an effective path average factor r where

$$r = \bar{R}/R_p$$

where $\bar{R}$ is path averaged rain rate and R_p is the surface-point

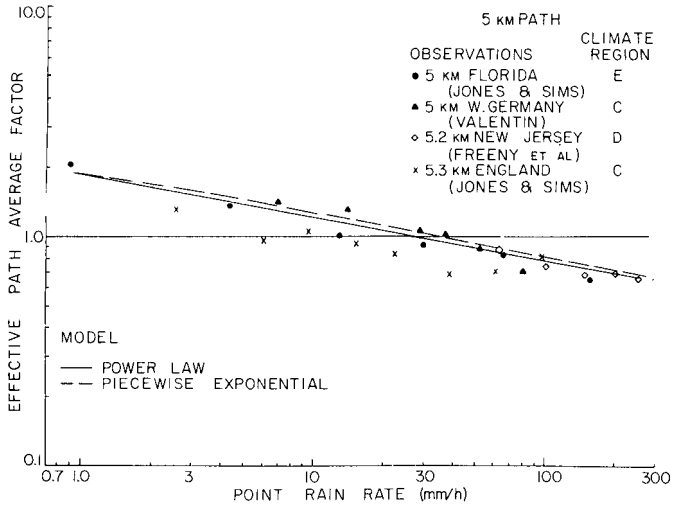

Fig. 9. Path averaged rain rate observations and point-to-path model.

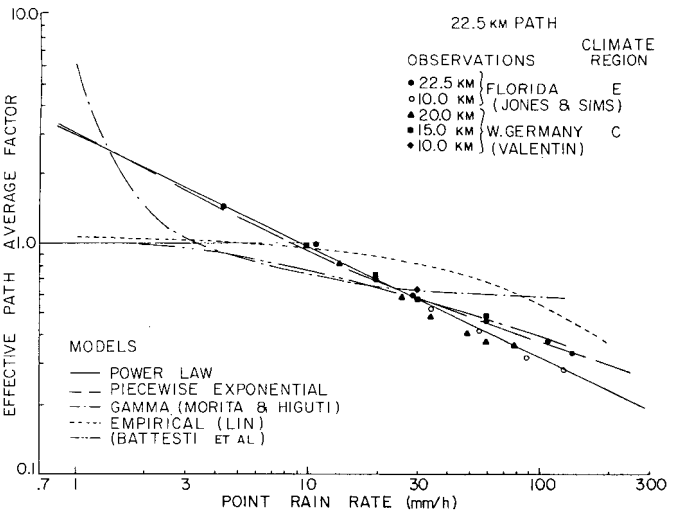

Fig. 10. Path averaged rain rate observations transformed to a 22.5 km path using the spatial independence assumption and model estimates.

rain rate. The data from Florida, New Jersey, and West Germany form an approximate power law relationship; the power law curve is the median of these data. Data for other observation path lengths also displayed approximate power law relationships.

Data were analyzed for path lengths of 5, 10, and 22.5 km. To obtain a sufficient sample size at 22.5 km, it was assumed that, for point rate rates in excess of 25 mm/h, their occurrence probabilities were independent over distances greater than 10 km. This is a reasonable assumption based upon experience with weather radar data. The assumption also produced agreement between observations at path lengths of 10, 15, 20, and 22.5 km and with the power law approximation as displayed in Fig. 10. In using the independence assumption, the path integrated rain rate value ($\bar{R}D$) for a path of length D_2 is equal to the value for a path of length D_1 when the exceedence probability is adjusted by the relative lengths of the paths:

$$P(\bar{R}_1 D_1) = P(\bar{R}_2 D_2) \cdot \left[\frac{D_1}{D_2}\right], \qquad \bar{R}D = \bar{R}_1 D_1 = \bar{R}_2 D_2 \tag{1}$$

where $P(\bar{R}D)$ is the probability of $\bar{R}$ being exceeded on a path of length D and the subscripts identify the path.

The power law relationship parameters were empirically established for distances from 0 to 22.5 km. The power law is expressed by

$$r = \gamma(D) R_p^{\,\delta(D)}; \quad \bar{R} = rR_p = \gamma R_p^{\,(1+\delta)} \tag{2}$$

where $\gamma(D)$ is given in Fig. 11(a) and $\delta(D)$ in Fig. 11(b). For paths D longer than 22.5 km, the value $\bar{R}D = rR_pD$ is identical to the $r'R_p'D_0$ value for a $D_0 = 22.5$ km path, but the R_p' value to be used for the 22.5 km path calculation is obtained from the rain rate distribution function at the probability of occurrence P', $P' = (22.5/D) \cdot P$ where P is the probability of interest.

This path average model produces the desired relationship between the rain rate at a point and the rain rate averaged over a horizontal path of length D. The specific attenuation, however, is a nonlinear function of point rain rate; hence, the model is not adequate for the estimation of attenuation. A statistical model of the profile of instantaneous rain rate along the path is required which then can be integrated to produce the desired attenuation value.

The simplest path profile for rain rate which, when integrated produces the observed median power law relationship, is the derivative of the power law relationship with respect to path length. The data in Fig. 11 were numerically differentiated to obtain this simplest profile model. The results are presented in Fig. 12. These data display the expected behavior. At high point rain rates, the intense rain occurs close to the origin or sampling point location. At low point rain rates, higher rain rates are more likely at distances in excess of 6 km from the sampling location. The latter value is half the average spacing between significant cells observed by Crane [18]. The path profile is still not in a form useful for attenuation modeling because it cannot be readily incorporated into an integral expression for attenuation. This last step is accomplished by a piecewise representation of the curves (Fig. 12) by exponential functions. An adequate model results when two exponential functions are used to span the 0-22.5 km distance range, one from 0 to d km, the other from d to 22.5 km. The resultant model for attenuation (or path integrated rain rate) is given by

$$A(R_p, D) = \alpha R_p^{\,\beta}\left[\frac{e^{u\beta d} - 1}{u\beta} - \frac{b^\beta e^{c\beta d}}{c\beta} + \frac{b^\beta e^{c\beta D}}{c\beta}\right];$$

$$d \leqslant D \leqslant 22.5 \text{ km}$$

$$A(R_p, D) = \alpha R_p^{\,\beta}\left[\frac{e^{u\beta D} - 1}{u\beta}\right]; \qquad 0 < D \leqslant d \tag{3}$$

where A is in dB, R_p in mm/h, the specific attenuation in

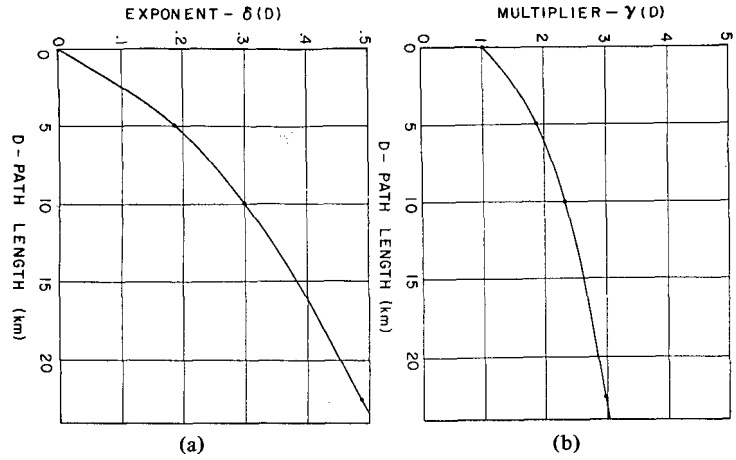

Fig. 11. (a) Multiplier in power law point-to-path model. (b) Exponent in power law point-to-path model.

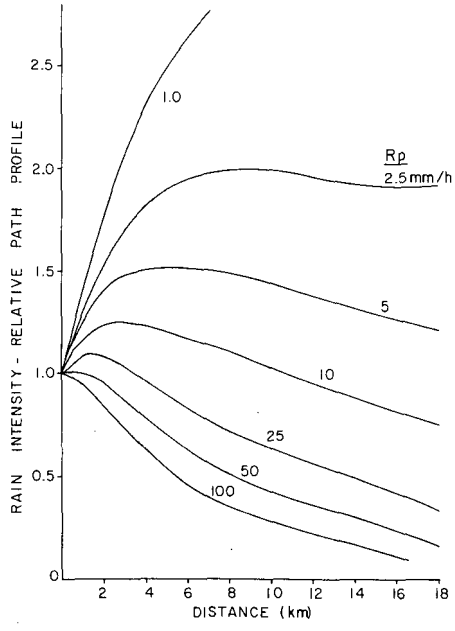

Fig. 12. Relative path rain rate profile, power law model.

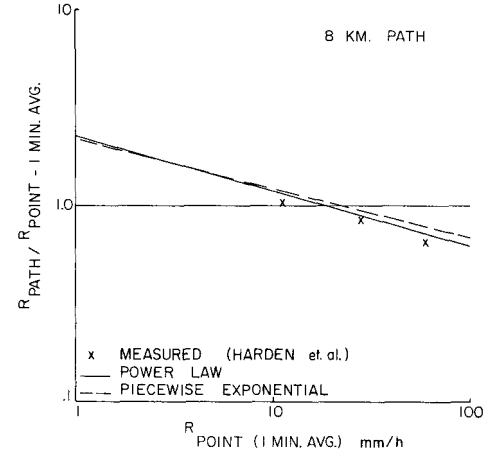

Fig. 13. Comparison between observations and model for data from the United Kingdom (after Harden *et al.* [28]).

dB/km is related to point rain rate by αR^{β} [32], and the remaining coefficients are empirical constants of the piecewise exponential model,

$$u = \frac{\ln [be^{cd}]}{d}; \qquad d \text{ in km} \tag{4}$$

$$b = 2.3\, R_p^{-0.17}; \qquad R_p \text{ in mm/h} \tag{5}$$

$$c = 0.026 - 0.03 \ln R_p \tag{6}$$

$$d = 3.8 - 0.6 \ln R_p. \tag{7}$$

The expression for path attenuation reduces to an expression for the path integrated rain rate when $\alpha = \beta = 1$. The use of this model for the estimation of the effective path average factor is illustrated by the dashed curves in Figs. 9 and 10.

A number of other path average models have been developed using either simultaneous attenuation observations [6], [7] or an assumed Gamma distribution and the observed spatial correlation properties between point rain gauge observations to model the rain rate distribution [31]. Several of these models are also displayed in Fig. 10. With the exception of the Gamma distribution model, the models do not portray the increase in the effective path average factor shown by the data at low rain rates. The Gamma distribution does not adequately represent the observed dependence of effective path average factor on point rain rate at rain rates below 20 mm/h.

Harden *et al.* [28], in their consideration of attenuation estimation for terrestrial communication systems, presented the results of additional point-to-path conversion measurements which were not used in the development of the power law and piecewise exponential models. Their data are presented in Fig. 13 together with the model predictions. The power law model predicts the experimental results with 10 percent of the observed values; the piecewise exponential model is within 20 percent. On the basis of the variations of all the observations including those used for the preparation of the model and other observations that have since become available, the piecewise exponential model will predict the observed path average rain rate given the equal exceedence

probability point rain rate with an rms uncertainty of 17 percent.

IV. PREDICTION OF THE VERTICAL VARIATION OF SPECIFIC ATTENUATION

The point-to-path model predicts the variation of rain rate along a horizontal (surface) path and is suitable for use in the design of terrestrial communication systems. For slant paths, the variation of specific attenuation in the vertical is also important. Theoretical analyses indicate that frozen precipitation in the form of ice and snow do not produce significant attenuation [10]. Water, when present in the form of raindrops or water coatings on raindrop size ice particles, produces significant attenuation.

At one time, the bright band or so-called melting layer evident in radar observations of widespread rain was thought to be caused by melting snow modeled as large water-coated snow particles that could produce significant attenuation [11]. Recent linearly polarized radar measurements of the change in cross section with the orientation of the polarization vector indicate that the bright band is in a region that is still predominantly snow, and that significant melting takes place below the bright band and at a height near the 0°C isotherm [33]. Microphysical observations further suggest that the bright band is produced by snowflake aggregation at about −2°C, and the melting process produces small liquid droplets at the extremities of the snowflakes which subsequently enlarge until the flake collapses into a raindrop. In this version of the melting process, increased attenuation due to large, uniformly wet structures will not occur; the attenuation will be proportional to the melted portion of the snow liquid water content until the larger collapsed drop is formed, at which time the theoretical specific attenuation, rain rate relationship obtains. The simultaneous radar and attenuation observations reported by McCormick [12] and by Goldhirsh [13] support the contention that only the melted raindrops produce attenuation and the regions of ice, snow, and aggregated snow crystals (bright band) do not cause significant amounts of attenuation.

Radar observations also show that rain is characterized on the average by a constant reflectivity from the surface to the height of the 0°C isotherm [15]. Based upon drop size distribution analyses, the constancy of the reflectivity value implies constancy in the value of specific attenuation. A useful model for the vertical structure of specific attenuation therefore assumes a constant value from the surface to the height of the 0°C isotherm. The specific attenuation value is deduced from the surface-point rain rate using a theoretically derived relationship based upon the analysis of drop size distribution data [32], [34].

The height of the 0°C isotherm varies with meteorological conditions. The seasonally and zonally averaged (averaged in longitude at a constant latitude) height of the 0°C isotherm varies from 4.7 km in the tropics to 3.1 km at 40° latitude to the surface at 61° latitude [35]. The height of the 0°C isotherm displays a marked seasonal dependence which, when coupled with the seasonal variation in the occurrence of the higher rain rates, indicates that the 0°C height to be used for the prediction of attenuation should have both a latitude and probability of occurrence dependence.

The dependence of the 0°C isotherm height on latitude and general rain conditions was established for seven locations within the United States using upper air sounding data, surface maps to establish the occurrence of precipitation, and excessive precipitation data to establish the correlation between 0°C height and the occurrence of excessive precipitation events. A high correlation between the average 0°C height and the height at which liquid raindrops exist should not be expected for the higher rain rates because large liquid water droplets are carried aloft above the 0°C height in the strong updraft cores of intense rain cells. Large drops can often be observed up to heights corresponding to temperatures near −5°C. As a model for the prediction of attenuation, the average height of the 0°C isotherm for days with rain was taken to correspond to the height to be expected 1 percent of the year. The highest height observed with rain was assumed to correspond to the value to be expected 0.001 percent of the year. Since the latter value corresponds to the average summer height of the −5°C isotherm, additional support is gained for its use. The latitude dependences of the heights to be expected for surface-point rain rates exceeded 1 percent of the year and 0.001 percent of the year were obtained from the latitude dependences provided by Oort and Rasmussen [35]. The resultant curves are presented in Fig. 14. For the estimation of model uncertainty, the seasonal rms uncertainty in the 0°C isotherm height was 500 m or roughly 13 percent of the average estimated height. The value of 13 percent is used to estimate the expected uncertainties to be associated with Fig. 14.

The correspondence between the 0°C isotherm height values and the excessive precipitation events showed a tendency toward a linear relationship between R_p and H where H is the 0°C isotherm height for high values of R_p. Since, at high rain rates, the rain rate distribution function displays a nearly linear relationship between R_p and $\log P$ (P is probability), the interpolation model used for the estimation of H for P between 0.001 and 1 percent is assumed to have the form

$$H = a + b \log P. \tag{8}$$

This relationship was used to provide the intermediate values displayed in Fig. 14.

The complete model for the estimation of attenuation on a slant path starts with the determination of the vertical distance between the height of the earth station and the 0°C isotherm height ($H - H_0$ where H_0 is station height) for the percentage of the year (or R_p) of interest. The surface projection of the path between the surface and the 0°C isotherm is used to calculate D:

$$\begin{aligned} D &= (H - H_0)/\tan\theta; \qquad \theta \geq 10^\circ \\ &= E\psi, \quad \psi \text{ in radians}; \quad \theta < 10^\circ \end{aligned} \tag{9}$$

where

$$\psi = \sin^{-1}\left[\frac{\cos\theta}{(H+E)} \cdot \left(\sqrt{(H_0+E)^2\sin^2\theta + 2E(H-H_0)+H^2-H_0^2} - (H_0+E)\sin\theta\right)\right]$$

E is the effective earth's radius (8500 km) and θ is the elevation angle.

The surface-projected attenuation is calculated from (3), and finally, the value for the slant path A_s is estimated using the constancy of specific attenuation below H by

$$A_s = \frac{LA(D)}{D} \tag{10}$$

where

$$L = D/\cos\theta;\ \theta \geq 10^\circ$$
$$= \sqrt{(E+H_0)^2 + (E+H)^2 - 2(E+H_0)(E+H)\cos\psi};\ \theta < 10^\circ.$$

V. PREDICTION OF VARIATION ABOUT THE ESTIMATED VALUE

The expected value of attenuation to be exceeded a specified percentage of the year is obtained from a four-step procedure requiring: 1) the estimation of the surface-point rain rate, 2) the specific attenuation given the point rain rate, 3) the physical extent of the attenuating region, and 4) the attenuation along the path. The procedure is empirical in nature; each step utilizes a median value derived from a pooled set of observations. The uncertainties claimed for each step are likewise empirical, being obtained from the observed variance of the pooled data. The uncertainties are summarized and combined in this section to provide an overall estimate of the uncertainty in attenuation prediction. The values are expressed as percentages and are to be used for all rain climate regions.

The rain rate climate regions were initially established to span a 40 percent range in rain rate between the empirical distribution functions for adjacent regions at a specified probability value. Distribution functions were pooled from each region to establish the median values of the distribution function at specified probability levels. The standard deviations of the distribution function values were independently obtained at selected probability levels from excessive precipitation data and from the observations reported by Harden *et al.* [28] for climate Region *C*. The resultant standard deviation estimates for the distribution function were 30 percent (in rain rate) at 0.001 and 1.0 percent of the year and 20 percent at 0.01 and 0.1 percent of the year. As an independent evaluation of the uncertainty estimate, the mean and standard deviation of the pooled region D_2 distribution functions were calculated at 0.01 percent of the year. The resultant values were 53 mm/h and 24 percent for the mean and standard deviation (as percent of mean), respectively. These values are in good agreement with the 49 mm/h and 20 percent model values.

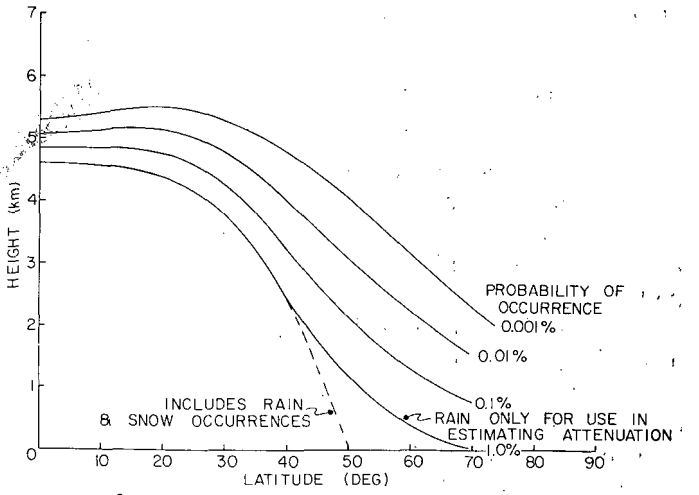

Fig. 14. 0°C isotherm height for use in estimating the depth of the attenuating region on a slant path.

The value of specific attenuation used in the model calculations is obtained from the point rain rate value using a power law relationship to approximate computations employing the Laws and Parsons drop size distribution [32], [34], [36]. Crane [10] found that differences between calculated values of specific attenuation obtained from the Laws and Parsons distribution and from a large number of observed drop size distributions were not statistically significant for frequencies up through 50 GHz. At higher frequencies, the drop size distribution measurement errors in the small drop size range, characteristic of currently available disdrometers, affects the accuracy of the specific attenuation, rain rate relationship. At frequencies up through 50 GHz, the power law relationship matches the calculations based on the Laws and Parsons distribution within an uncertainty of five percent over the 0.25–150 mm/h rain rate range of interest. The additional uncertainties associated with sampling the drop size distribution are negligible and may be ignored [10].

The physical extent of the attenuating region is defined without any uncertainty for a terrestrial path, but depends upon the vertical extent of the rain region for a slant path. In the latter case, the standard deviation associated with the estimate of rain region height was 13 percent.

The point-to-path relationship was obtained from a median best fit curve to the observed variation of the effective path average factor with point rain rate for data pooled from three separate rain climate regions. The data show statistical variation (Figs. 9 and 10) about the piecewise exponential model curve. The spread is associated with both the intrinsic variability of the relationship within and between climate regions and the statistical uncertainties in the estimate of the distribution functions used for the calculation of the effective

TABLE II
EXPECTED STANDARD DEVIATION OF MEASUREMENTS ABOUT MODEL IN PERCENT

Path Type \ Percent of Year	1	.1	.01	.001
Terrestrial Path	36	28	28	36
Slant Path	39	32	32	39

path average factor and point rain rate values due to the limited (a year or less) duration of the observations. Ignoring the latter problem, the data show a 17 percent (rms) deviation about the model curve.

In summary, the several steps of the attenuation prediction model are based on the use of median values of statistically variable quantities. The statistical processes associated with each step can be assumed to be independent of each other and the variances combined on that basis. The terms in the attenuation prediction equation (3) corresponding to each step are multiplicative; hence, we use the percent values for the standard deviations. The variances of the logarithms of the individual bounds were combined to produce the final variance estimate (again expressed in percent). The resultant standard deviation estimates are presented in Table II. These values apply to the estimate of the year-to-year variability in attenuation on a single path or within-the-region variability of similar paths.

VI. APPLICATION OF THE MODEL

Terrestrial Paths

The attenuation prediction model may be used for terrestrial or slant paths operating at any elevation angle. The model was developed solely on the basis of geophysical rain rate and rain structure data, not on the use of simultaneous attenuation observations. The utility of the model, however, can only be established by comparison with attenuation observations.

Harden *et al.* [28] reported on the variation of observed attenuation distributions with distance at fixed percentage of occurrence values obtained on a number of terrestrial paths in the UK. These data are depicted in Figs. 15-17 for frequencies of 11.0, 20.0, and 36.5 GHz, respectively. Two model results are presented: one for the rain rate distribution for rain climate Region *C*, the other for the average measured rain rate distribution R_p (Fig. 8). In calculating the attenuation values, the α and β coefficients in Figs. 18 and 19 and Table III were used. These values were obtained for a Laws and Parsons [36] drop size distribution and a 0°C drop temperature using the procedure described by Crane [34].

At 11.0 GHz, the data are clustered about the model curves for 0.01 percent of the year and about the model results based upon the use of the average measured distribution at 0.001 percent of the year. The one standard deviation bounds (from Table II) are plotted about the model calculation made using the average measured rain rate distribution. Seventy percent of the observations are within the one standard deviation bounds at 0.01 percent of the year, 90 percent at 0.001 percent of the year. These results show excellent agreement between prediction and calculation based on the average ob-

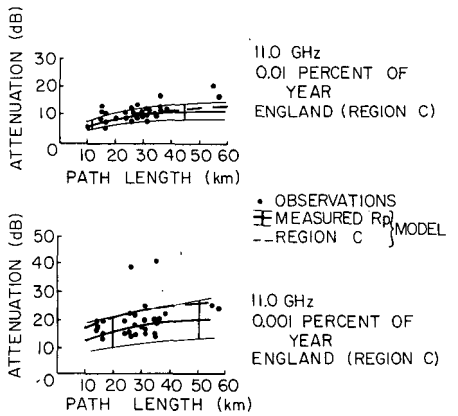

Fig. 15. Terrestrial path observations at 11.0 GHz in the United Kingdom [28].

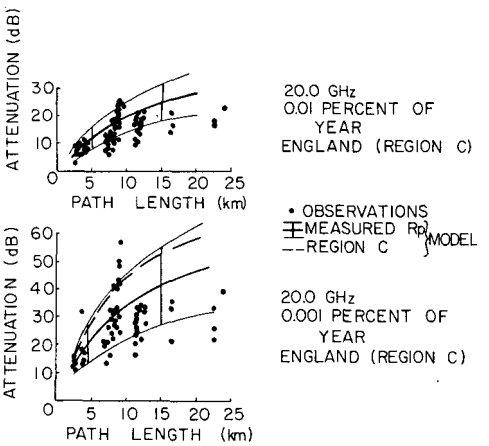

Fig. 16. Terrestrial path observations at 20.0 GHz in the United Kingdom [28].

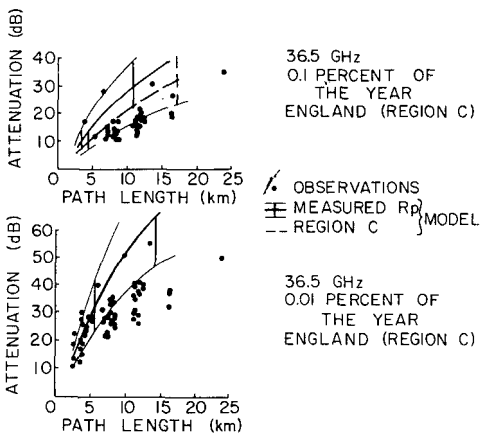

Fig. 17. Terrestrial path observations at 36.5 GHz in the United Kingdom [28].

served rain rate distribution. The observed variation about the model calculation is caused by the within-region change in the rain rate distribution. The model calculations using the climate Region *C* rain rate distribution are also in good agreement with the observations; 70 percent of the observations are within the one standard deviation bounds at 0.01 percent of the year and 59 percent are within the bounds at 0.001 percent of the year. The model does well at all distances well into

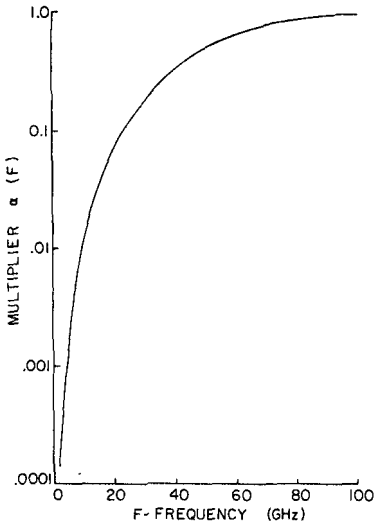

Fig. 18. Multiplier in the power law relationship between specific attenuation and frequency.

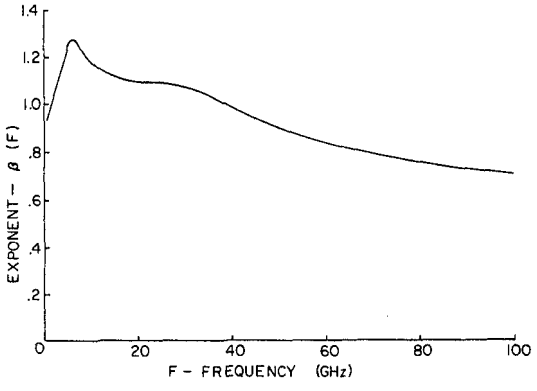

Fig. 19. Exponent in the power law relationship between specific attenuation and frequency.

TABLE III
PARAMETERS FOR COMPUTING SPECIFIC ATTENUATION
$a = \alpha R_p^{\beta}$ (dB/km)

Frequency F - GHz	Multiplier α(F)	Exponent β(F)
1	0.00015	0.95
4	0.00080	1.17
5	0.00138	1.24
6	0.00250	1.28
7.5	0.00482	1.25
10	0.0125	1.18
12.5	0.0228	1.145
15	0.0357	1.12
17.5	0.0524	1.105
20	0.0699	1.10
25	0.113	1.09
30	0.170	1.075
35	0.242	1.04
40	0.325	0.99
50	0.485	0.90
60	0.650	0.84
70	0.780	0.79
80	0.875	0.753
90	0.935	0.730
100	0.965	0.715

the region requiring the application of the independence assumption of Section III. It is noted that the measurements and model agree at a frequency where the nonlinearity in the αR^{β} relationship is relatively important.

At 20 GHz (Fig. 16) reasonable agreement is again evident between the model calculations employing the average measured rain rate distribution R_p. At 0.01 percent of the year, 68 percent of the observations are within one standard deviation of the model prediction (using either R_p or climate Region C); at 0.001 percent of the year, 71 percent are within the one standard deviation bound for the model employing R_p, but only 45 percent are within the bounds for calculations based on the use of the rain climate C distribution. At 0.001 percent of the year, all the out-of-bounds points relative to the Region C calculation show less attenuation than predicted, a result consistent with the difference between R_p and the Region C curve shown in Fig. 8. In general, the impression gained from Fig. 16 is a tendency for the model to underestimate the attenuation for longer paths, a result that could be due to a limited dynamic range of the observing equipment.

At 36.5 GHz, the rain climate Region C distribution curve provides a better fit to the observations; at 0.1 percent of the year, 51 percent of the obervations are within the one standard deviation bounds of the climate Region C curve, while only 14 percent are within the plotted bounds about the R_p calculation. In this case, the rain climate region model provides a better match to the observations. Again, the effect of poor instrument dynamic range is evident at the longer ranges. At 0.01 percent of the year, 78 percent of the observations are within the plotted bounds for paths with lengths shorter than 6 km or expected attenuation values less than 30 dB; 55 percent are within bounds for ranges less than 10 km; but only two observations (11 percent) are within bounds for ranges greater than 10 km (observations which require dynamic ranges in excess of 50 dB).

Measurements on paths having an expected attenuation values of less than 30 dB show excellent agreement between model prediction and observation, particularly when reliable rain rate distribution estimates are available. The success of the prediction method did not depend upon path length for the data shown except where attenuation values in excess of 30 dB are expected. These results confirm the use of the model on terrestrial paths.

Slant Paths

Recent observations using the CTS, COMSTAR, and ATS-6 satellite beacons allow the evaluation of the model at a number of frequencies and locations in Regions D_2 and D_3 of the United States. An example of observations of CTS at 11.7 GHz [37] together with model predictions is given in Fig. 20. The observations match (within 1 dB) the Region D_2 model between 0.2 and 1.0 percent of the year and are within the one standard deviation bounds of the Region D_2 model for percentages of the year less than 0.03. Since agreement between measurements and model calculations is best expressed on a percentage basis, the data are replotted in Fig. 21. The measurements show generally good agreement with the model

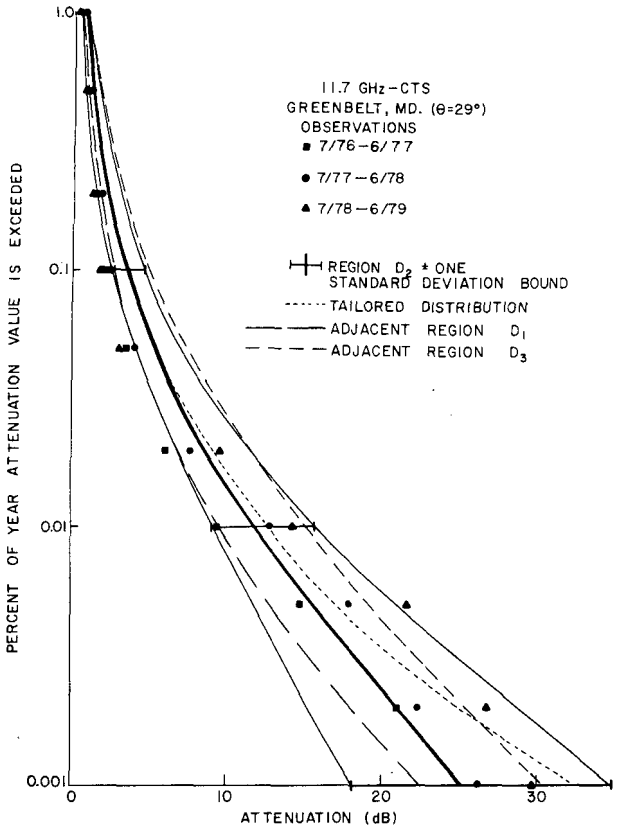

Fig. 20. Slant path observations at 11.7 GHz (after Ippolito [37]).

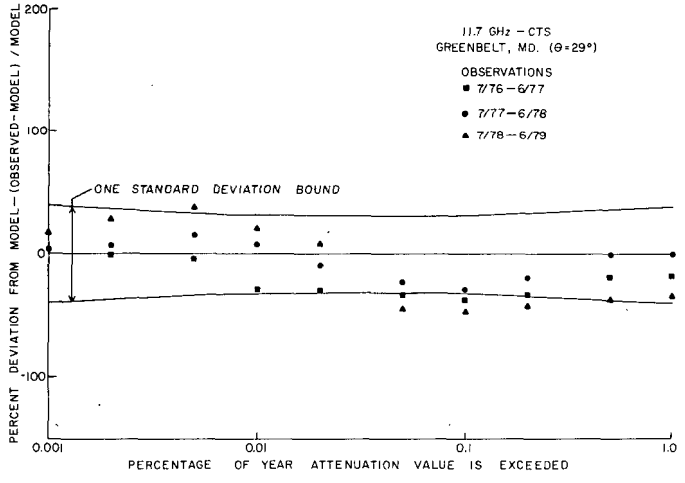

Fig. 21. Slant path observations as percent deviation from the model estimate; same data as Fig. 20.

predictions; 79 percent of the observations lie within the one standard deviation bounds shown in the figure.

Comparisons between a larger sample of observations and model calculations are presented in Fig. 22. The data presented in this figure include the comparison already presented in Fig. 21 plus 11.7 GHz CTS observations from Waltham, MA [38] (see Fig. 4 for location), Holmdel, NJ [39], Blacksburg, VA [8], and Austin, TX [40]; 19.04 and 28.56 GHz–COMSTAR observations from Holmdel, NJ [41], Clarksburg, MD [42], Wallops Island, VA [43], and Blacksburg, VA [8]; and 20 and 30 GHz–ATS-6 measurements from Rosman, NC

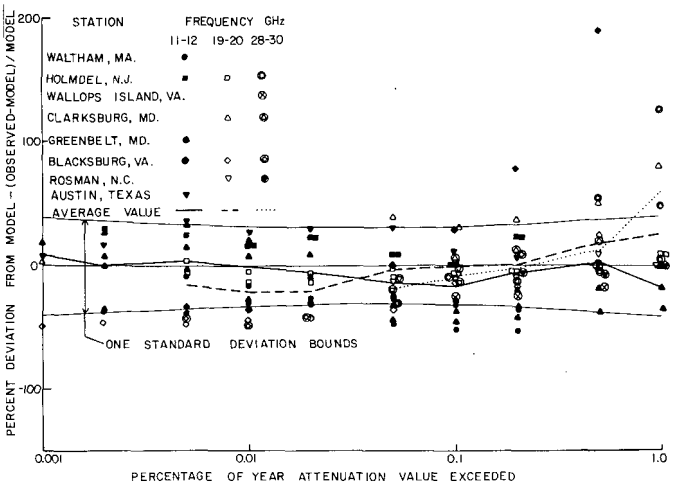

Fig. 22. Slant path observations as percent deviation from the model estimate for seven locations and three frequencies. The locations are given in Fig. 4.

[44]. These data show excellent agreement between measurement and model for percentages of the year less than 0.1 and for all percentages at locations other than Blacksburg, VA. For all the data plotted in Fig. 22, 76 percent of the observations were within the one standard deviation bound about the model prediction. The model is also well supported on average as shown in Fig. 23. In this figure, the mean deviation and standard deviation of the measurements about model predictions are displayed for the data averaged (over frequency and years) at each observation site. The mean deviation is not statistically different from zero (at one standard deviation), indicating that the model predicts attenuation without bias. The standard deviation of the observations about the model is also in good agreement with the predicted value.

Elevation Angle Dependence

The slant path attenuation model provides attenuation estimates for all elevation angles. The sun tracker observations made in the early 1970's provide data for comparison with elevation angle dependence estimates. Kinase and Kinpara [45] provided data on the elevation angle variation of 11.7 GHz attenuation observations for Klang, Malaysia (climate Region *H*; see Fig. 6). The model calculations for 10 and 20 mm/h (0.66 and 0.33 percent of the year, respectively) are presented as a function of elevation angle in Fig. 24 together with the observations for the same probabilities of exceedence. The model results and measurements show definite departures from a simple cosecant of the elevation angle dependence at both high and low elevation angles. The model agrees with observation at the rms deviation expected for observations which vary in elevation angle in synchronism with the sun (~53 percent rms). The data for all elevations and both probabilities of occurrence have a 48 percent rms deviation about the model predictions; at elevation angles above 10°, the rms deviation is less than 36 percent.

These data show excellent agreement between the prediction model and observations.

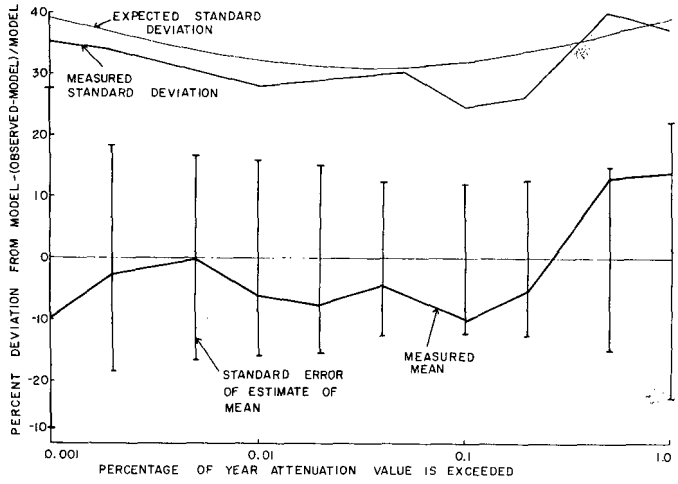

Fig. 23. Mean and standard deviation of the differences between observation and prediction averaged (over time and frequency) at each site.

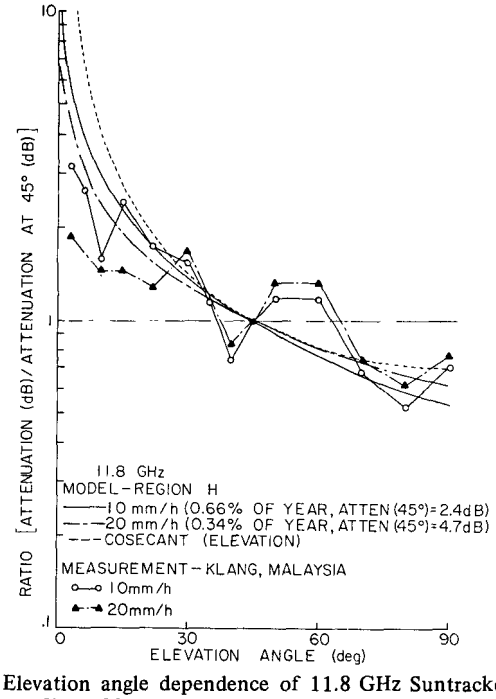

Fig. 24. Elevation angle dependence of 11.8 GHz Suntracker observations at Klang, Malaysia (climate region H; after Kinase and Kinpara [45]).

VII. CONCLUSIONS

A new model for the prediction of attenuation due to rain for use on either terrestrial or slant propagation paths has been prepared and tested against terrestrial system measurements from paths of different length and satellite observations on slant paths of differing elevation angle. For measurements of acceptable quality, the measurements and predictions agree within the predicted one standard deviation bounds for measurements about the model. The average behavior of the predictions is also excellent; the mean deviations between measurement and model are smaller than 14 percent.

The model provides both the outline of a general prediction procedure and a set of detailed steps for making a prediction. The step-by-step procedure is summarized in the Appendix. The model was developed for easy application; the results presented in this paper were all obtained by the author's teenage daughter using a pocket calculator.

Some of the steps in the model deserve additional consideration. The model for the 0°C isotherm height was generated using data from a limited number of upper air stations in the United States, all of which have station heights within 300 m of mean sea level. The model was extended globally on the basis of zonal averages. Application has been successful for stations in low mountains near the coast, but no consideration was made of the general modification of the vertical tempera ture structure caused by large regions of high terrain such as the high plains of Kansas or other similar regions.

Additional refinement in the rain rate climate description is also possible, but requires high quality data spanning more than 10 years at each location. More work is also required on understanding the local variations in rain rate climate, but again, long duration records are required for analysis. Noting the assumed correspondence between measurements made at one point in space over a long time period and over a larger spatial area over much shorter periods, say of a year or two, well-calibrated weather radar observations may provide the data required to extend the model and establish the effects of local terrain variations.

The model should be extended to provide seasonal and monthly predictions. For many system applications, the problem is to establish the design for the worst month to be expected in a number of years. A useful definition of a worst month has been established [46], but the procedures presented in this paper must be modified and expanded to provide a means to estimate worst month performance statistics.

APPENDIX

STEP-BY-STEP APPLICATION OF THE ATTENUATION PREDICTION MODEL

Step 1—Determine Rain Rate Distribution R_p.

1a) Locate path endpoints (terrestrial) or earth station on map (Figs. 3 or 4) and determine rain climate region, A-H.

1b) Obtain rain rate distribution from Table I (or Fig. 5 or 7).

Note that a tailored distribution may be prepared for special locations (see text) and in some instances measured distributions may be available. Caution is recommended in the use of measured instantaneous (1 min average) rain rate distributions if the observations are for a period of less than 10 years.

Step 2—Establish Surface Projected Path Length D.

2a) For terrestrial paths, D is the separation between antennas.

2b) For slant paths, the distance D is calculated from

$$D = (H(P) - H_0)/\tan\theta; \qquad \theta \geq 10^\circ$$

$$= E\psi, \text{ see (9)}; \qquad \theta < 10^\circ$$

where θ is the elevation angle, H_0 is the station height, and $H(P)$ is the 0°C isotherm height obtained by interpolation in Fig. 14 for the percentage of time P of interest. To interpolate, plot $H(P)$ versus log P and use a straight line to relate H to log P.

2c) If $D > 22.5$ km, use both $D_0 = 22.5$ km and a new point rain rate R_p' for the modified probability of occurrence,

$$P' = P\left[\frac{D_0}{D}\right]$$

for subsequent calculations.

Step 3–Determine α and β for the frequency of interest from Table II or Figs. 18 and 19.

Step 4–Calculate the surface projected attenuation value A from the R_p and D (or R_p' and D_0). R_p is the rain rate obtained from the rain rate distribution for the probability of occurrence of interest P:

$$A(R_p, D) = \alpha R_p{}^{\beta}\left[\frac{e^{u\beta d} - 1}{u\beta} - \frac{b^{\beta}e^{c\beta d}}{c\beta} + \frac{b^{\beta}e^{c\beta D}}{c\beta}\right]; \qquad d \leqslant D \leqslant D_0$$

$$A(R_p, D) = \alpha R_p{}^{\beta}\left[\frac{e^{u\beta D} - 1}{u\beta}\right]; \qquad D < d$$

$$A(R_p, D) = (H(P) - H_0)\alpha R_p{}^{\beta}; \qquad D = 0(\theta = 90°)$$

where

$$u = \frac{\ln\left[be^{cd}\right]}{d},$$

$$b = 2.3\, R_p{}^{-0.17},$$

$$c = 0.026 - 0.03 \ln R_p, \quad \text{and}$$

$$d = 3.8 - 0.6 \ln R_p.$$

Step 5–Adjust for height along a slant path (do not perform this step for terrestrial application).

See (10) for $\theta < 10°$:

$$A_s = \frac{LA(R_p, D)}{D} = \frac{A(R_p, D)}{\cos\theta}; \qquad \theta \geqslant 10°$$

where A_s is the slant path attenuation.

ACKNOWLEDGMENT

The measurements used for model evaluation were made available to the author by contractors working for NASA, by Bell Laboratories, and by GTE. The author wishes to acknowledge the help of D. Blood in the preparation of the manuscript and of his daughter, Kathy, who calculated the slant path attenuation estimates during a vacation from high school.

REFERENCES

[1] R. K. Crane, "Propagation phenomenon affecting satellite communication systems operating in the centimeter and millimeter wavelength bands," *Proc. IEEE*, vol. 59, pp. 173–188, 1971.

[2] ——, "Attenuation due to rain—A mini review," *IEEE Trans. Antennas Propagat.*, vol. AP-23, pp. 750–752, 1975.

[3] P. L. Rice and N. R. Holmberg, "Cumulative time statistics of surface-point rainfall rates," *IEEE Trans. Commun.*, vol. COM-21, pp. 1131–1136, 1973.

[4] W. C. Y. Lee, "An approximate method for obtaining rain rate statistics for use in signal attenuation estimating," *IEEE Trans. Antennas Propagat.*, vol. AP-27, pp. 407–413, 1979.

[5] E. J. Dutton and H. T. Dougherty, "Year-to-year variability of rainfall for microwave applications in the USA," *IEEE Trans. Commun.*, COM-27, pp. 829–832, 1979.

[6] J. Battesti, L. Boithias, and P. Misme, "Determination de l'affaiblissement dēs a la pluie pour les frequences superieures a 10 GHz," *Ann des Telecommun.*, vol. 26, pp. 439–444, 1971.

[7] S. H. Lin, "Nationwide long-term rain statistics and empirical calculation of 11 GHz microwave rain attenuation," *Bell Syst. Tech. J.*, vol. 56, pp. 1581–1604, 1977.

[8] W. L. Stutzman and C. W. Bostian, "A millimeter wave attenuation and depolarization experiment using the COMSTAR and CTS satellite," Final Rep. SATCOM-79-2, Virginia Polytechnic Inst. and State Univ., Blacksburg, VA; U.S. Army Res. Office, Grant PAAG 29-77-G-0083, 1979.

[9] R. R. Rogers, "Statistical rainstorm models: Their theoretical and physical foundations," *IEEE Trans. Antennas Propagat.*, vol. AP-24, pp. 547–566, 1976.

[10] R. K. Crane, "Prediction of the effects of rain on satellite communication systems," *Proc. IEEE*, vol. 65, pp. 456–474, 1977.

[11] J. R. Joss, R. Cavalli, and R. K. Crane, "Good agreement between theory and experiment for attenuation data," *J. de Recherches Atmosph.*, vol. 8, pp. 299–318, 1974.

[12] K. S. McCormick, "A comparison of precipitation attenuation and radar backscatter along earth-space paths," *IEEE Trans. Antennas Propagat.*, vol. AP-20, pp. 745–755, 1972.

[13] J. Goldhirsh, "Predictive methods for rain attenuation using radar and in-situ measurements tested against the 28-GHz COMSTAR beacon signal," *IEEE Trans. Antennas Propagat.*, vol. AP-27, pp. 398–406, 1979.

[14] T. W. Harrold and P. M. Austin, "The structure of precipitation systems—A review," *J. de Recherches Atmosph.*, vol. 8, pp. 41–57, 1974.

[15] J. Goldhirsh and I. Katz, "Useful experimental results for earth-satellite rain attenuation modeling," *IEEE Trans. Antennas Propagat.*, vol. AP-27, pp. 413–415, 1979.

[16] W. F. Bodtmann and C. L. Ruthroff, "Rain attenuation on short radio paths: Theory, experiment, and design," *Bell Syst. Tech. J.*, vol. 53, pp. 1329–1349, 1974.

[17] H. E. Bussey, "Microwave attenuation statistics estimated from rainfall and water vapor statistics," *Proc. IRE*, vol. 38, pp. 781–785, 1950.

[18] R. K. Crane, "Automatic cell detection and tracking," *IEEE Trans. Geosci. Electron.*, vol. GE-17, pp. 250–262, 1979.

[19] L. J. Ippolito, "11.7 GHz attenuation and rain rate measurements with the Communications Technology Satellite (CTS)," NASA Tech. Memo. 80283, NASA/Goddard Space Flight Center, Greenbelt, MD, 1979.

[20] D. M. A. Jones and A. L. Sims, "Climatology of instantaneous rainfall rates," *J. Appl. Meteorol.*, vol. 17, pp. 1135–1140, 1978.

[21] R. C. Barry and R. J. Chorely, *Atmosphere, Weather, and Climate*. New York: Holt, Rinehart, and Winston, 1970.

[22] CCIR, "Radiometeorological data," CCIR Study Group 5 Rep. 563-1 ITU, Geneva, Switzerland, 1978.

[23] E. J. Dutton, "Precipitation variability in the U.S.A. for microwave terrestrial system design," OTR77-134, NTIS, Springfield, VA, 1977.

[24] H. E. Landsberg, Ed., *World Survey of Climatology*, Vols. 1–15. Amsterdam, The Netherlands: Elsevier, 1974.

[25] B. Haurwitz and J. Austin *Climatology*. New York: McGraw-Hill, 1944.

[26] M. S. V. Rao, W. V. Abbott, III, and J. S. Theon, "Satellite-derived global oceanic rainfall atlas (1973 and 1974)," NASA-SP-410 NASA/Goddard Space Flight Center, Greenbelt, MD, 1976.

[27] H. L. Crutcher and O. M. Davis, "U.S. Navy Marine climate atlas of the World, vol. VIII," NAVAIR 50-1C-54, Naval Weather Service Command, U.S. Navy, 1969.
[28] B. N. Harden, J. R. Norbury, and W. J. K. White, "Estimation of attenuation by rain on terrestrial radio links in the UK at frequencies from 10 to 100 GHz," *Microwave, Optics and Acoustics*, vol. 2, pp. 97–104, 1978.
[29] A. E. Freeny and J. D. Gabbe, "A statistical description of intense rainfall," *Bell Syst. Tech. J.*, vol. 48, pp. 1789–1851, 1969.
[30] R. Valentin, "Statistiken der Regendämpfung für Richtfunkverbindungen uber 10 GHz," Deutsche Bundespost Forschungsinstitet beim FTZ, Rep. 455-TB-62, 1977.
[31] K. Morita and I. Higuti, "Statistical studies in electromagnetic wave attenuation due to rain," *Rev. Elect. Comm. Lab. (Japan)*, vol. 19, pp. 798–842, 1971.
[32] R. L. Olsen, D. V. Rogers, and D. B. Hodge, "The aR^b relation in the calculation of rain attenuation," *IEEE Trans. Antennas Propagat.*, vol. AP-26, pp. 318–329, 1978.
[33] R. K. Crane, "Evaluation of uncertainties in the estimation of hydrometeor mass concentrations using SPANDAR data and aircraft measurements," Scientific Rep. 1., Environmental Res. Tech., Inc., Air Force Contract F19628-76-C-0069; AFGL-TR-78-0018, Air Force Geophys. Lab., Hanscom AFB, MA, 1978.
[34] R. K. Crane, "Microwave scattering parameters for New England rain," Tech. Rep. 426, Massachusetts Inst. Tech. Lincoln Lab., Lexington, MA, 1966.
[35] A. H. Oort and E. M. Rasmusson, *Atmospheric Circulation Statistics*, NOAA Professional Paper 5, U.S. Dept. of Commerce, 1971.
[36] J. O. Laws and D. A. Parsons, "The relation of raindrop-size to intensity," *Am. Geophys. Union Trans.*, vol. 24, pp. 452–460, 1943.
[37] L. J. Ippolito, private communication, 1979.
[38] D. Nackoney, "CTS 11.7 beacon data," Tech. Note TN78-471.3, GTE Lab., Inc., 1978.
[39] A. J. Rustako, Jr., "Measurement of rain attenuation and depolarization of the CTS satellite beacon signal at Holmdel, New Jersey," USNC-URSI Meeting, Seattle, WA, abstract only, 1979.
[40] W. J. Vogel, "CTS attenuation and cross polarization measurements at 11.7 GHz," Final Rep. Cont. NAS5-22576, Elec. Eng. Res. Lab., Univ. of Texas at Austin, Austin, TX, 1979.
[41] H. W. Arnold, D. C. Cox, H. H. Hoffman, and R. P. Leck, "Rain attenuation statistics from a 19 and 28 GHz COMSTAR beacon propagation experiment: One year cumulative distributions and relationships between two frequencies," *IEEE Trans. Commun.*, 1979.
[42] J. M. Harris and G. Hyde, "Preliminary results of COMSTAR 19/29 GHz beacon measurements at Clarksburg, Maryland," *COMSAT Tech. Rev.*, vol. 7, pp. 599–623, 1977.
[43] J. Goldhirsh, "Cumulative slant path rain attenuation statistics associated with the COMSTAR beacon at 28.56 GHz for Wallops Island, Virginia," *IEEE Trans. Antennas Propagat.*, vol. AP-27, 1979.
[44] L. J. Ippolito, "20 and 30 GHz millimeter wave experiments with ATS-6 satellites," NASA TND-8197, NASA Goddard Space Flight Center, Greenbelt, MD, 1976.
[45] A. Kinase and A. Kinpara, "Statistics of attenuation due to precipitation of radio waves in 12 GHz band at higher angles of elevation," Note 101, NHK Tech. Res. Labs., Tokyo, Japan, 1973.
[46] R. K. Crane and W. E. Debrunner, "Worst month statistics," *Electron. Lett.*, vol. 14, pp. 38–40, 1978.

★

Robert K. Crane (SM'71–F'80) received the B.S., M.S., and Ph.D. degrees in electrical engineering from Worcester Polytechnic Institute, Worcester, MA.

He was employed by The MITRE Corporation, where he worked on radar inputs to the SAGE system and on the effects of refraction on radar measurement accuracy. He then became a staff member of the M.I.T. Lincoln Laboratory where he conducted basic and applied research on radio wave propagation through the ionosphere and lower atmosphere, the structure of precipitation systems, and on turbulence in the clear atmosphere. He also served as principal investigator on programs to investigate bistatic scattering from rain and the statistics of weather radar echos conducted for NASA. Other experience includes the observation and analysis of the effects of rain, atmospheric turbulence, and ionospheric irregularities on radar, microwave radiometer, and satellite communication systems. During 1970, 1971 and 1974, he was a U.S. delegate to the International Radio Consultative Committee (CCIR) Meetings and to the World Administrative Radio Conference in 1971 as a Propagation Specialist. He is presently Division Senior Scientist, Earth Resources and Atmospheric Physics Division, Environmental Research & Technology, Inc. (ERT), Concord, MA. He is responsible for remote sensing studies of the earth's atmosphere, basic research in cloud physics, weather modification, radar meteorology, clear air turbulence, atmospheric dynamics, and basic research in radio wave propagation through the atmosphere.

Dr. Crane is a member of the American Meteorological Society, the American Geophysical Union, the International Union of Radio Science (Commission F), Sigma Xi, and Eta Kappa Nu.